Scanning Microwave Microscopy for Biological Applications: Introducing the State of the Art and Inverted SMM

Scanning Microwave Microscopy for Biological Applications

Marco Farina,[1,a)] and James C. M. Hwang[2]

[1]*Dept. of Information Engineering, Università Politecnica delle Marche, 60131 Ancona, Italy*

[2]*Dept. of Materials Science and Engineering, Cornell University, Ithaca, NY 14853 USA*

[a)] E-mail: m.farina@univpm.it

I. OLD HAT OF SUBWAVELENGTH MICROSCOPY

Often a student comes into my office excited by a revolutionary idea! I invite him or her to check the literature carefully. In particular, check it way back, even for more than a century. For example, encouraged by Albert Einstein, Edward H. Synge introduced in 1928 the concept of a near-field scanning microscope in the paper "A suggested method for extending microscopic resolution into the ultra-microscopic region" [1]. He claims to have overcome the "…axiom in microscopy, that the only way to extend resolving power lies in the employment of light of smaller wavelength." For subwavelength resolution of a biological sample, he proposes to place within 10 nm of the sample an opaque screen with a pinhole of 10-nm diameter (Fig. 1). Light passing through the pinhole and the sample is focused on a photodetector. By moving the screen laterally in 10-nm steps, the sample is imaged with 10-nm resolution, regardless of the wavelength of the light. Later, what he proposes is known as a scanning near-field optical microscope (SNOM).

As mentioned by Synge, Ernst K. Abbe stated in 1873 that the best possible resolution of a traditional microscope is approximately half of the light wavelength [2]. Why doesn't Abbe's axiom apply to an SNOM? Imagine a conductivity probe tracing across a metal sample that is grounded. When the probe falls off the metal edge, the conductivity drops sharply. How sharp the conductivity drops depends only on how sharp the probe is, even though it is a DC measurement of effectively an infinite wavelength. If, instead of a DC measurement, an AC signal is applied to the probe, the probe can interact capacitively with the sample even without touching it. How sharply an AC probe resolves the metal edge can again be a function of the probe sharpness. It requires only that the probe be kept within a tiny fraction of the wavelength of the sample, so that the capacitive interaction is quasi-static and limited to a range comparable to the probe sharpness.

For an SNOM, the biggest challenge is the precise movement of the screen. Synge overcame this challenge by using two quartz crystals to move the screen piezo-electrically with nanometer precision [3]. Remarkably, piezoelectric scanners are still used in near-field scanning microscopes today. I can't help smiling when I find his estimate of how long it takes to scan an image is so close to what I struggle with in the lab every day. Equally remarkably, all of Synge's work was forgotten before Ash and Nicholls demonstrated in 1972 near-field sub-wavelength imaging [4]. This inspired not only Binnig and Rohrer's Nobel Prize-winning development of the scanning tunneling microscope (STM) in 1982 [5], but also the rediscovery of Synge's papers. Finally, he is vindicated for inventing the general concept of near-field scanning microscopy, and, in particular, SNOM.

In a modern scanning-probe microscope, instead of a screen with a pinhole, a sharp stylus is scanned across a sample while recording the near-field interaction. The interaction can result in a tunneling current in an STM, or a contact force in an atomic force microscope (AFM) [6]. A scanning-probe microscope is often operated in a closed-loop mode with a feedback mechanism to keep the interaction constant. In this mode, the vertical movement of the piezoelectric scanner, required to keep the tunneling current or the atomic force constant, closely follows the sample topography. This is why a scanning microwave microscope (SMM), the newest scanning-probe microscope, is usually based on an STM or AFM to control the probe at a fixed height above the sample.

II. Atomic Resolution Despite Centimeter-long Wavelength

In an SMM, the near-field interaction is electromagnetic. With capacitive coupling, an SMM does not need to touch the sample, which avoids many of the pitfalls of a contacting probe. For example, the SMM probe does not deform soft samples like biological cells. Once a physiology expert asked me why cells all appear so smooth in an AFM, not realizing that it is similar to using a heavy iron to feel wrinkled clothes. A contacting probe is constantly wiped clean as it scans a hard sample, but can gather dust on a soft sample. A contacting probe can form an electrical junction with the sample, so the measured conductivity is complicated by the junction characteristics.

Why microwaves? A low-frequency AC signal can sense capacitive coupling without contact. However, for a sample size of 10-nm square, the coupling capacitance can be as small as an attofarad (10^{-18} F). Since the conductance through a capacitor increases linearly with frequency, the higher the frequency, the smaller the capacitor that can be sensed. This is why it is possible to use an SMM to sense the electromagnetic properties of a sample with atomic resolution [7]-[10].

Unlike an STM or AFM, an SMM can sense below the surface [11]-[14]. This is because the microwave signal emitted from the SMM probe can penetrate a dielectric sample up to one micrometer. With subsurface sensitivity, atomic resolution, noncontact probing, and decades of development, SMMs have been successfully used to image semiconductors doped on the surface [15] or in the interior [16], surface acoustic waves [17], topological insulators [18], and quantum spin Hall edges [19], all of which is beyond what can be done with AFM, STM or SNOM.

SMM has another important advantage over SNOM in terms of noninvasiveness. This is because the energy of a microwave photon is several orders of magnitude less than the energy of a visible photon. This is especially critical to biological samples as visible light is known to cause side effects such as optogenetics [20],

photobleaching [21], and phototoxicity [22]. Additionally, SNOM usually requires a biological sample to be labeled with a fluorescent dye, which can change the properties of the sample, whereas SMM doesn't require labeling. Finally, SMM can reveal critical electromagnetic properties of a biological sample. For example, the electrical impedance has been shown to be different in live vs. dead cells [23], healthy vs. cancerous cells [24], and normal vs. fatigued bloods [25].

III. Microwaving Biological Samples Without Hurting Them

Despite being noninvasive, label-free, and sensitive to subsurface electromagnetic impedance, biological applications remain challenging for SMM. First, cells need to be kept alive in a saline-like medium, which can absorb the microwave signal and cause parasitic capacitive coupling [26]. (AFM and STM are not better off, because AFM can force a cell to swim and STM can conduct through the medium. In comparison, the higher the frequency, the less conductive a cell-culture medium is [27]. Ions are slowpokes at microwave frequencies.) Until a decade ago, there had been few examples of bio-SMM and they were mostly on rigid or dead tissues. For example, human bone osteons and tooth cavities were detected in 1999, as shown in Fig. 2 [28]. The wall and cytoplasm of yucca cells were delineated and the shape of blood vessels in pig ribs were resolved in 2005 [29]. The cell and synaptic structures of a dissected fruit fly's antennal lobe and the ommatidial clusters of its compound eyes were imaged in 2007 [30].

Over the past decade, SMM has finally been getting its feet wet in testing live cells and organelles quantitatively! In 2011, the frequency was raised from about 1 GHz to about 10 GHz into the true microwave range, and submicron resolution was demonstrated on a dried human monocytic leukemia cell [31]. In 2015, using a carbon-nanotube probe in the tapping mode, the nucleus and cytoplasm of a dried corneal endothelial cell were delineated [32]. In 2016, dried human osteoblast-like cells were imaged [33], but the different microwave responses from subcellular structures such as cytoplasm and organelles may be dominated by topographic crosstalk [34]. With removal of topographic crosstalk and calibration *in situ* [35], [36], the dielectric constant of dried *E. coli* bacteria was quantified to be around 4 [37]–[39]. Dried DNA in a microarray were observed [40]. Live yeast cells adhering to a membrane were imaged through the membrane, which prevents the cell suspension from wetting the SMM probe [41]. A vital mitochondrion isolated from human cancer cells was imaged in a respiration medium, as shown in Fig. 3 [42].

Over the past decade, we have actively supported this dry-to-wet and qualitative-to-quantitative development, especially in enabling SMM to work on a live cell in a saline-like medium and in quantifying its electromagnetic properties. In 2012, we used SMM tomography [12]-[14] to highlight how a carbon nanotube is incorporated in a dried mouse muscle cell [43]. Although the round shape of the nanotube is revealed by the AFM, the higher microwave absorption of the nanotube interior can only be seen by the SMM. This study was followed in 2015 with the use of an STM-based broadband SMM to image dried mouse myofibrils and rabbit sarcomeres [44]. The long STM probe minimizes topographic crosstalk. Broadband SMM allows post-processing of the frequency-domain data after Fourier transformation to the time domain for optimum gating and signal-to-noise ratio [45]. Fig. 4 compares the mouse myofibril images from STM and SMM. The benefit of time-gated SMM is evident.

In 2016, we used the same STM-based broadband SMM to confirm that the impedance of a dried human breast cancer cell varies with its incorporation of fullerene [46]. Fullerene is an allotrope of carbon with a lipophilic cage structure of sixty atoms capable of delivering drugs and other molecules inside a cell. Fig. 5 shows an SMM image of a cell and its impedance as a function of fullerene exposure. Similar to fullerenes, exosomes are messengers between cells and can be isolated from human saliva, for example. (Similar to the COVID-19 virus!) Using the same STM-based broadband SMM with time-gated signal processing, we imaged dried exosomes smaller than 100 nm with higher contrast and resolution than was possible using STM or AFM [47]. This shows that, in addition to STM and AFM, SMM can be complementary to other techniques in identifying exosomes such as dynamic light scattering, nanoparticle tracking analysis, electron microscopy, surface plasmon resonance, and immunoaffinity capture [48]. In 2018, we increased the SMM frequency into the millimeter-wave range (50 GHz) for improved sensitivity (Sec. II) to a mitochondrion [49]. The mitochondrion is isolated from myogenic cells of human gluteus media muscle, then dried on highly oriented pyrolytic graphite. Broadband measurement is performed to allow time gating around 8.57 ns. Fig. 6(c) shows that the resulting image reveals cristae in the mitochondrion, which are not visible in either our STM image or the SMM image of Fig. 4 [42].

In 2019, we had both hardware and software breakthroughs which enabled SMM of unprecedented image quality and signal-to-noise ratios [50]. Broadband measurement with hundreds of frequencies from 1 to 9 GHz is possible even for an AFM-based SMM. For the first time, images of 128 × 128 pixels over 201 frequencies can be acquired in approximately 20 min, fast enough for imaging of a live cell. Beyond imaging, for removal of topographic crosstalk and measurement of electromagnetic properties in a saline-like medium, the previous *in situ*

calibration technique [35], [36] is extended in liquid [27] through a combination of analytical and numerical models [51]. Fig. 7 shows the evolution of a rat myoblast cell in a culture medium 2.5-mm deep. The bottom of the petri dish is lined with an indium-tin-oxide transparent conductor to allow *in situ* calibration, cell adhesion, and optical microscopy. Fluorescence microscopy confirms that, despite repeated SMM imaging, cells remain viable for more than 10 h. The relative permittivity of the center of the cell on top of its nucleus is quantified as $(32 \pm 6) - j\,(20 \pm 4)$, which is in general agreement with the literature and simple estimation. It is also close to the dielectric constant of 15–30 estimated for a dried *E. coli* bacterium in 40% humidity [38].

Because it combines noninvasiveness with subsurface sensitivity, SMM has great potential for continuous monitoring of the physiological condition of a live cell at the subcellular level. To achieve this potential, however, the SMM scan rate needs to be further increased through both hardware and software improvements. For continuous monitoring, the number of pixels may be reduced, although currently it is difficult for the SMM probe to remain on the same spot of a live cell, even with the cell adhering to the substrate. Similarly, the resonance frequency of a live cell may drift, so some form of broadband SMM is desirable. Otherwise, one never knows whether the SMM signal is changed by the physiological state of a cell or by extrinsic resonance factors. Not all biological experiments require atomic resolution. The probe tip size is a trade-off between sensitivity, noninvasiveness, and spatial resolution. SMM, a new and complicated instrument, needs to be carefully optimized both mechanically and electrically. Nevertheless, great progress has been made over the past decade in applying the SMM to live biological samples. Even more rapid progress can be expected over the next decade.

IV. Turning the SMM World Upside Down

Also in 2019, we proposed a Copernican paradigm shift called the inverted SMM (iSMM) [52]. Fig. 8 shows that in an iSMM, the probe is always grounded and the microwave signal is injected through the sample from a slot line or other forms of a transmission line. The probe can be a simple, rugged, and bio-compatible metal stylus. According to the reciprocity theory of electromagnetics, the *intrinsic* interaction between the probe tip and the sample is the same whether the microwave signal is injected through the probe or the sample. However, the *extrinsic* parasitic interaction is drastically different. In iSMM, with the microwave signal injected through the sample and the probe grounded, the parasitic interaction between the probe body and the surround is greatly reduced, because most of the surround is grounded. Note that for a well-shielded conventional SMM probe, the intrinsic signal from the sample is often masked by the parasitic interaction between the probe body and the surround and suffers from strong

topographic crosstalk [38]. Unlike a conventional SMM probe, the iSMM transmission line can have a broadband impedance match over many decades of frequency. The input and output of the transmission line are connected to the VNA, so that both reflection and transmission coefficients are measured. Such a two-port measurement usually has a dynamic range of 120–140 dB, whereas the conventional one-port SMM measurement has a dynamic range of 40–60 dB. This makes resonance or interference setup unnecessary for sensing the tiny perturbance when the probe scans across the sample, allowing broadband measurement for time gating and tomography. Thus, an iSMM can be conveniently built from any scanning probe microscope, such as an AFM or STM, with a simple metal probe and a custom sample holder, and will outperform a conventional SMM in terms of ruggedness, bandwidth, sensitivity, and dynamic range.

The iSMM has been demonstrated on dried human lymphocyte cells and live rat myocyte cells [52]. The iSMM images formed by the transmission coefficient are significantly better than the images of the two-port conventional SMM [54], [17]. With greatly reduced parasitic interaction, the iSMM reliably quantifies the dielectric constant as 2.8 ± 0.7 uniformly across a dried rat myocyte cell [52] and 2.6 ± 0.3 across a dried human lymphocyte cell [53], results that are comparable to that of lipid bilayers in electrolyte solution but lower than that of dried E. coli bacteria [38]. Fig. 9 compares the AFM topography and SMM dielectric-constant images of a human lymphocyte cell. It can be seen that the dielectric constant is uniform across the cell, independent of topography.

The above examples are for an iSMM converted from an AFM-based SMM. For an STM-based SMM, the iSMM conversion may enable it to be used on live cells by controlling the leakage current in a saline-like medium through an electrochemical cell. It remains to be seen whether or not the iSMM can indeed turn the SMM world upside down. It may take a century to prove another revolutionary idea.

References

[1] E. H. Synge, “XXXVIII. A suggested method for extending microscopic resolution into the ultra-microscopic region,” *Philos. Mag.*, vol. 6, no. 35, p. 356–362, Aug. 1928.

[2] E. Abbe, “Beiträge zur theorie des mikroskops und der mikroskopischen wahrnehmung,” *Arch. Mikrosk. Anat. Entwicklungsmech.*, vol. 9, pp. 413–418, 1873.

[3] E. H. Synge, “XXIII. An application of piezo-electricity to microscopy,” *Philos. Mag.*, vol. 13, no. 83, pp. 297–300, Feb. 1932.

[4] E. A. Ash and G. Nicholls, “Super-resolution aperture scanning microscope,” *Nature*, vol. 237, no. 5357, pp. 510–512, Jun. 1972.

[5] G. Binnig, H. Rohrer, Ch. Gerber, and E. Weibel, “Surface studies by scanning tunneling microscopy,” *Phys. Rev. Lett.*, vol. 49, no. 1, pp. 57–61, Jul. 1982.

[6] G. Binnig, C. F. Quate, and Ch. Gerber, “Atomic force microscope,” *Phys. Rev. Lett.*, vol. 56, no. 9, pp. 930–933, Mar. 1986.

[7] D. E. Steinhauer, C. P. Vlahacos, S. K. Dutta, B. J. Feenstra, F. C. Wellstood, and S. M. Anlage, "Quantitative imaging of sheet resistance with a scanning near-field microwave microscope," *Appl. Phys. Lett.,* vol. 72, no. 7, p. 861, Feb. 1998.

[8] X.-D. Xiang and C. Gao, "Quantitative complex electrical impedance microscopy by scanning evanescent microwave microscope," *Mater. Charact.,* vol. 48, no. 2/3, pp. 117–125, Apr. 2002.

[9] B. Hu, W. Liu, C. Gao, X. Zhu, and D. Zheng, "Quantitative microscopy of nonlinear dielectric constant using a scanning evanescent microwave microscopy," *Appl. Phys. Lett.,* vol. 89, no. 4, p. 044102, Jul. 2006.

[10] J. Lee, C. J. Long, H. Yang, X.-D. Xiang, and I. Takeuchi, "Atomic resolution imaging at 2.5 GHz using near-field microwave microscopy," *Appl. Phys. Lett.,* vol. 97, no. 18, p. 183111, Nov. 2010.

[11] M. Tabib-Azar and Y. Wang, "Design and fabrication of scanning near-field microwave probes compatible with atomic force microscopy to image embedded nanostructures," *IEEE Trans. Microw. Theory Techn.,* vol. 52, no. 3, pp. 971–979, Mar. 2004.

[12] C. Plassard *et al.,* "Detection of defects buried in metallic samples by scanning microwave microscopy," *Phys. Rev. B,* vol. 83, no. 12, p. 121409, Mar. 2011.

[13] G. Gramse *et al.,* "Quantitative sub-surface and non-contact imaging using scanning microwave microscopy," *Nanotechnol.,* vol. 26, no. 13, p. 135701, Mar. 2015.

[14] X. Jin *et al.,* "Scanning microwave microscopy of buried CMOS interconnect lines with nanometer resolution," *Int. J. Microwave Wireless Technol.,* vol. 10, no. 5/6, pp. 556–561, Jun. 2018.

[15] E. Brinciotti *et al.,* "Probing resistivity and doping concentration of semiconductors at the nanoscale using scanning microwave microscopy," *Nanoscale,* vol. 7, no. 35, pp. 14715–14722, Sep. 2015.

[16] G. Gramse *et al.,* "Nondestructive imaging of atomically thin nanostructures buried in silicon," *Sci. Adv.,* vol. 3, no. 6, p. e1602586, Jun. 2017.

[17] L. Zheng, D. Wu, X. Wu, and K. Lai, "Visualization of surface-acoustic-wave potential by transmission-mode microwave impedance microscopy," *Phys. Rev. Appl.,* vol. 9, no. 6, p. 061002, Jun. 2018

[18] S. S. Hong *et al.,* "Ultrathin topological insulator Bi_2Se_3 nanoribbons exfoliated by atomic force microscopy," *Nano Lett.,* vol. 10, no. 8, pp. 3118–3122, Aug. 2010.

[19] Y. Shi et al., "Imaging quantum spin Hall edges in monolayer WTe_2," *Sci. Adv.,* vol. 5, no. 2, p. eaat8799, Feb. 2019.

[20] C. P. O'Banion, and D. S. Lawrence, "Optogenetics: A primer for chemists," *Chem. Bio. Chem.,* vol. 19, no. 12, pp. 1201–1216, Jun. 2018.

[21] M. Atif, M. Zellweger, and G. Wagnieres, "Review of the role played by the photosensitizer's photobleaching during photodynamic therapy," *J. Optoelectron. Adv. Mater.,* vol. 18, no. 3/4, pp. 338–350, Apr. 2016.

[22] S. Goetze, C. Hiernickel, and P. Elsner, *Skin Pharmacol. Physiol.,* vol. 30, no. 2, pp. 76-80, May 2017.

[23] Y. Ning *et al.,* "Broadband electrical detection of individual biological cells," *IEEE Trans. Microw. Theory Techn.,* vol. 62, n. 9, pp. 1905–1911, Sept. 2014.

[24] J. Chen, J. Li, and Y. Sun, "Microfluidic approaches for cancer cell detection, characterization, and separation," *Lab Chip,* vol. 12, no. 10, pp. 1753–1767, Apr. 2012.

[25] R. Esfandyarpour, A. Kashi, M. Nemat-Gorgani, J. Wilhelmy, and R. W. Davis, "A nanoelectronics-blood-based diagnostic biomarker for myalgic encephalomyelitis/chronic fatigue syndrome (ME/CFS)," *Proc. Natl. Acad. Sci. USA,* vol. 116, no. 21, pp. 10250–10257, May 2019.

[26] M. Farina, A. Di Donato, D. Mencarelli, G. Venanzoni, and A. Morini, "High resolution scanning microwave microscopy for applications in liquid environment," *IEEE Microw. Compon. Lett.,* vol. 22, no. 11, pp. 595−597, Nov. 2012.

[27] X. Jin, M. Farina, X. Wang, G. Fabi, X. Cheng, and J. C. M. Hwang, "Quantitative scanning microwave microscopy of the evolution of a live biological cell in a physiological buffer," *IEEE Trans. Microw. Theory Techn.,* vol. 67, no. 12, pp. 5438–5445, Dec. 2019.

[28] M. Tabib-Azar, J. L. Katz, and S. R. LeClair, "Evanescent microwaves: a novel super-resolution noncontact nondestructive imaging technique for biological applications," *IEEE Trans. Instrum. Meas.,* vol. 48, no. 6, pp. 1111–1116, Dec. 1999.

[29] J. Park, S. Hyun, A. Kim, T. Kim, and K. Char, "Observation of biological samples using a scanning microwave microscope," *Ultramicroscopy,* vol. 102, no. 2, pp. 101–106, Jan. 2005.

[30] K. Lai, M. B. Ji, N. Leindecker, M. A. Kelly, and Z. X. Shen, "Atomic-force-microscope-compatible near-field scanning microwave microscope with separated excitation and sensing probes," *Rev. Sci. Instrum.,* vol. 78, no. 6, p. 063702, Jun. 2007.

[31] Y. J. Oh *et al.,* "High-frequency electromagnetic dynamics properties of THP1 cells using scanning microwave microscopy," *Ultramicroscopy,* vol. 111, no. 11, pp. 1625–1629, Nov. 2011.

[32] Z. Wu *et al.,* "Imaging of soft material with carbon nanotube tip using near-field scanning microwave microscopy," *Ultramicroscopy,* vol. 148, pp. 75–80, Jan. 2015.

[33] L. Zhang, Y. Song, A. Hosoi, Y. Morita, and Y. Ju, "Microwave atomic force microscope: MG63 osteoblast-like cells analysis on nanometer scale," *Microsyst. Technol.,* vol. 22, no. 3, pp. 603–608, Mar. 2016.

[34] S. M. Anlage, V. V. Talanov, and A. R. Schwartz, "Principles of near-field microwave microscopy," in *Scanning Probe Microscopy,* S. Kalinin and G. Gruverman, Ed. New York, NY, USA: Springer, 2007, pp. 215–253.

[35] M. Farina, D. Mencarelli, A. Di Donato, G. Venanzoni, and A. Morini, "Calibration protocol for broadband near-field microwave microscopy," *IEEE Trans. Microw. Theory Techn.,* vol. 59, no. 10, pp. 2769–2776, Oct. 2011.

[36] G. Gramse, M. Kasper, L. Fumagalli, G. Gomila, P. Hinterdorfer, and F. Kienberger, "Calibrated complex impedance and permittivity measurements with scanning microwave microscopy," *Nanotechnol.,* vol. 25, no. 14, p. 145703, Mar. 2014.

[37] S.-S. Tuca *et al.,* "Single E-coli bacteria imaged at 20 GHz frequency using the scanning microwave microscope (SMM)," *Microsc. Anal.,* vol. 29, no. 4, pp. 912, Aug. 2015.

[38] M. C. Biagi *et al.,* "Nanoscale electric permittivity of single bacterial cells at gigahertz frequencies by scanning microwave microscopy," *ACS Nano,* vol. 10, no. 1, pp. 280–288, Jan. 2016.

[39] S.-S. Tuca *et al.,* "Calibrated complex impedance of CHO cells and *E. coli* bacteria at GHz frequencies using scanning microwave microscopy," *Nanotechnol.,* vol. 27, no. 13, p. 135702, Apr. 2016.

[40] A. Babajanyan, B. Friedman, and K. Lee, "Nondestructive label-free mapping of DNA bioassay using a near-field scanning microwave microscope," *Arm. J. Phys.,* vol. 9, no. 2, pp. 148–153, May 2016.

[41] A. Tselev, J. Velmurugan, A. V. Ievlev, S. V. Kalinin, and A. Kolmakov, "Seeing through walls at the nanoscale: microwave microscopy of enclosed objects and processes in liquids," *ACS Nano,* vol. 10, no. 3, pp. 3562–3570, Mar. 2016.

[42] J. Li, Z. Nemati, K. Haddadi, D. C. Wallace, and P. J. Burke, "Scanning microwave microscopy of vital mitochondria in respiration buffer," in *IEEE MTT-S Int. Microwave Symp. (IMS) Dig.,* Jun. 2018, pp. 115–118.

[43] M. Farina *et al.,* "Tomographic effects of near-field microwave microscopy in the investigation of muscle cells interacting with multi-walled carbon nanotubes," *Appl. Phys. Lett.,* vol. 101, n. 20, p. 203101, Nov. 2012.

[44] M. Farina et al., "Imaging of biological structures by near-field microwave microscopy," in *Proc. European Microwave Conf. (EuMC),* Sept. 2015, pp. 666–669.

[45] M. Farina *et al.,* "Disentangling time in a near-field approach to scanning probe microscopy," *Nanoscale,* vol. 3, no. 9, pp. 3589–3593, Sep. 2011.

[46] M. Farina *et al.,* "Investigation of fullerene exposure of breast cancer cells by time-gated scanning microwave microscopy," *IEEE Trans. Microw. Theory Techn.,* vol. 64, no. 12, pp. 4823–4831, Dec. 2016.

[47] X. Jin *et al.,* "Imaging of exosomes by broadband scanning microwave microscopy," in *Proc. European Microwave Conf. (EuMC),* Oct. 2016, pp. 1211−1214.

[48] F. Piacenza *et al.,* "Measuring zinc in biological nanovesicles by multiple analytical approaches," *J. Trace Elem. Med. Biol.,* vol. 48, pp. 58−66, Mar. 2018.

[49] M. Farina *et al.,* "Imaging of sub-cellular structures and organelles by an STM-assisted scanning microwave microscope at mm-waves," in *IEEE MTT-S Int. Microwave Symp. (IMS) Dig.,* Jun. 2018, pp. 111−114.

[50] X. Jin, M. Farina, X. Wang, G. Fabi, X. Cheng, and J. C. M. Hwang, "Broadband scanning microwave microscopy of a biological cell with unprecedented image quality and signal-to-noise ratio," in *IEEE MTT-S Int. Microwave Symp. (IMS) Dig.,* Boston, MA, USA, Jun. 2019, pp. 216−219.

[51] X. Jin, J. C. M. Hwang, D. Mencarelli, L. Pierantoni, and M. Farina, "Nano probing for microwave engineers," *IEEE Microw. Mag.,* pp. 71–75, Jan./Feb. 2017.

[52] M. Farina *et al.,* "Inverted scanning microwave microscope for *in vitro* imaging and characterization of biological cells," *Appl. Phys. Lett.,* vol. 114, no. 9, p. 093703, Mar. 2019.

[53] G. Fabi, C. H. Joseph, X. Jin, X. Wang, J. C. M. Hwang, and M. Farina, "Electrical properties of Jurkat cells: an inverted scanning microwave microscope study," in *IEEE MTT-S Int. Microwave Symp. (IMS) Dig.,* Jun. 2020, pp. 1−4.

[54] A. O. Oladipo *et al.*, "Analysis of a transmission mode scanning microwave microscope for subsurface imaging at the nanoscale," *Appl. Phys. Lett.*, vol. 105, no. 13, p. 133112, Sep. 2014.

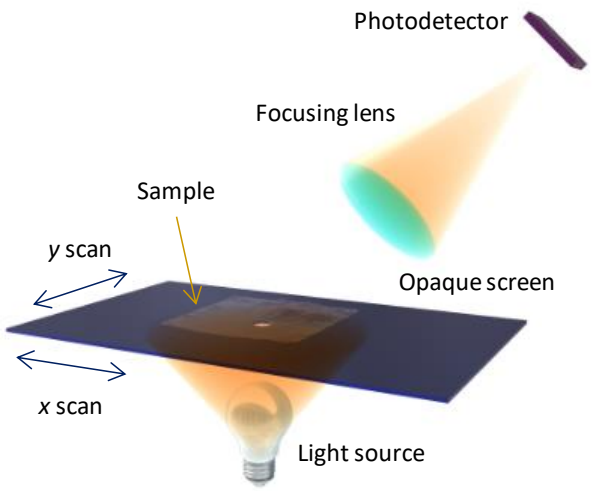

Fig. 1. Schematics of E. H. Synge's original concept of a scanning near-field optical microscope [1]. A light source is placed below an opaque screen with a pinhole. The sample is placed less than 10 nm above the screen. The screen is moved laterally in x and y directions. Light passing through the pinhole and the sample is focused on a photodetector. The microscope can image the sample with spatial resolution on the order of the hole size.

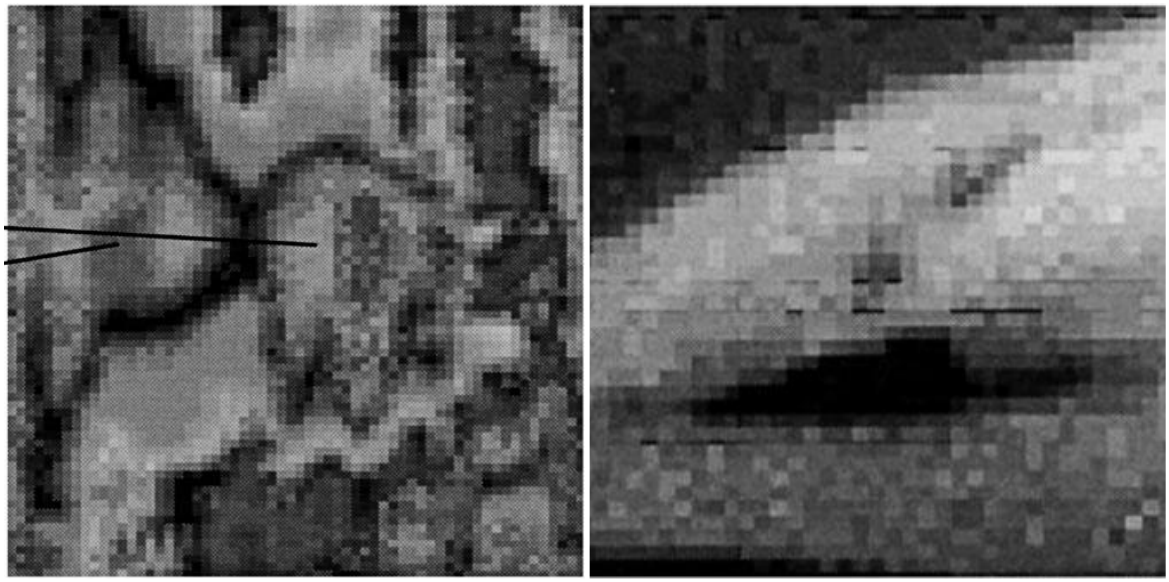

(a) (b)

Fig. 2. SMM cross-section images of (a) a human femoral cortical bone and (b) a human tooth with 10-μm resolution [28].

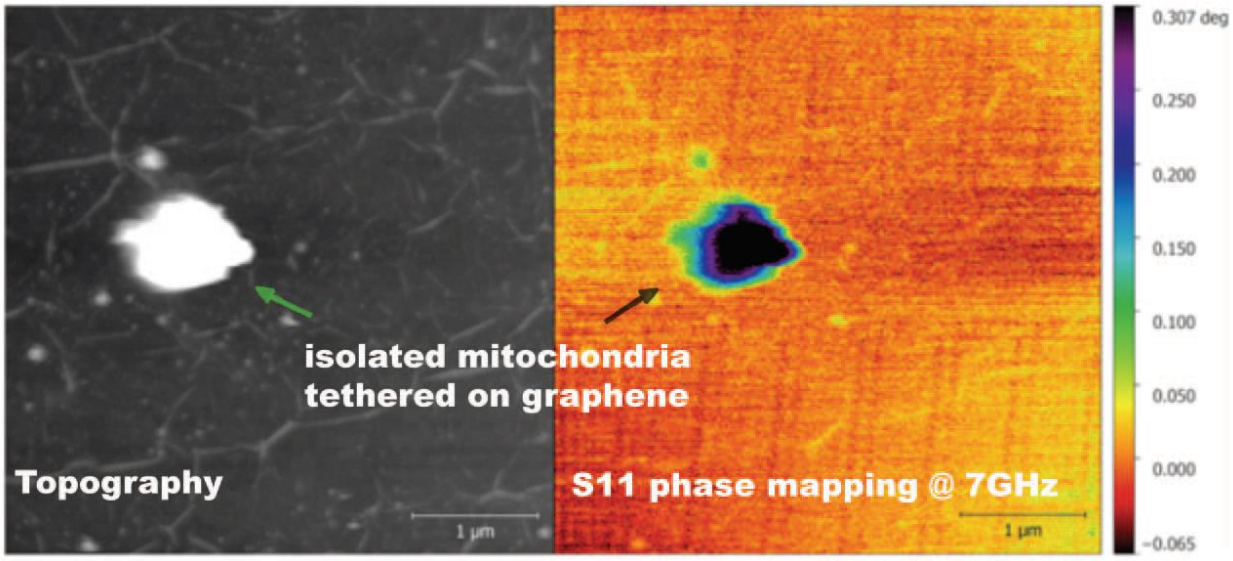

(a) (b)

Fig. 3. (a) AFM and (b) SMM images of a vital mitochondrion isolated from HeLa cell culture and tethered on graphene support [42].

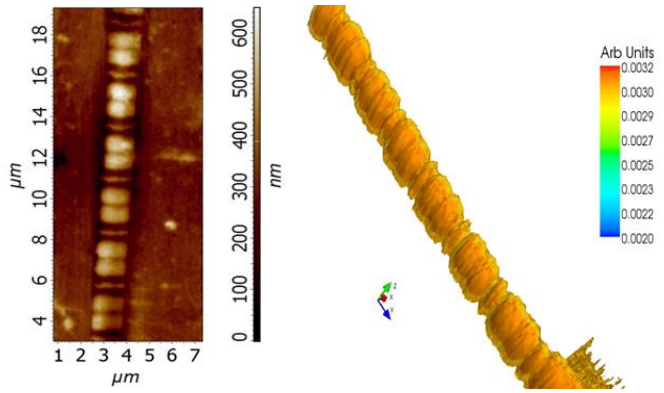

(a) (b)

Fig. 4. (a) STM and (b) SMM images of a mouse muscle myofibril showing the sarcomere bands [44]. The unit in (b) is dimensionless, as the microwave signal is converted from the frequency domain to the time domain.

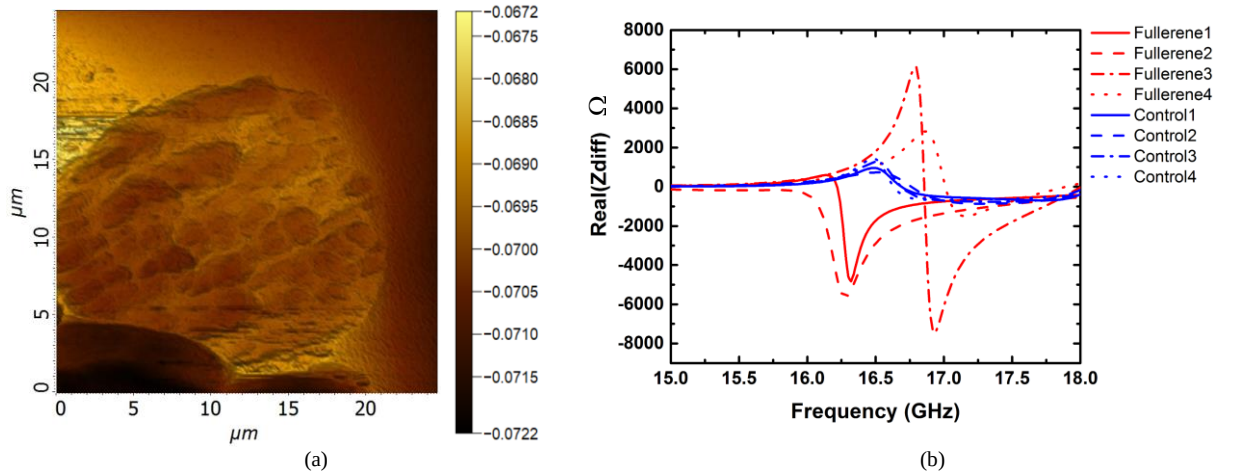

(a) (b)

Fig. 5. (a) SMM image of a MCF-7 human breast cancer cell and (b) its impedance variation with fullerene exposure [46]. In (b), four cells with different fullerene exposures were characterized by SMM and compared to another four unexposed cells of matching dimensions.

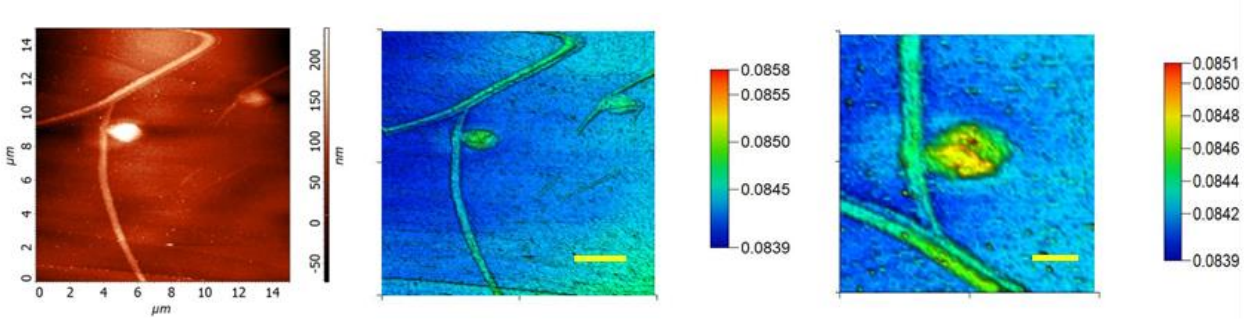

(a) (b) (c)

Fig. 6. (a) STM, (b) SMM, and (c) SMM detailed images of a mitochondrion in a layer of water and glucose [49]. Horizonal scale bar is 2 μm in (b) and 1 μm in (c). Vertical units in (b) and (c) are dimensionless in the time domain.

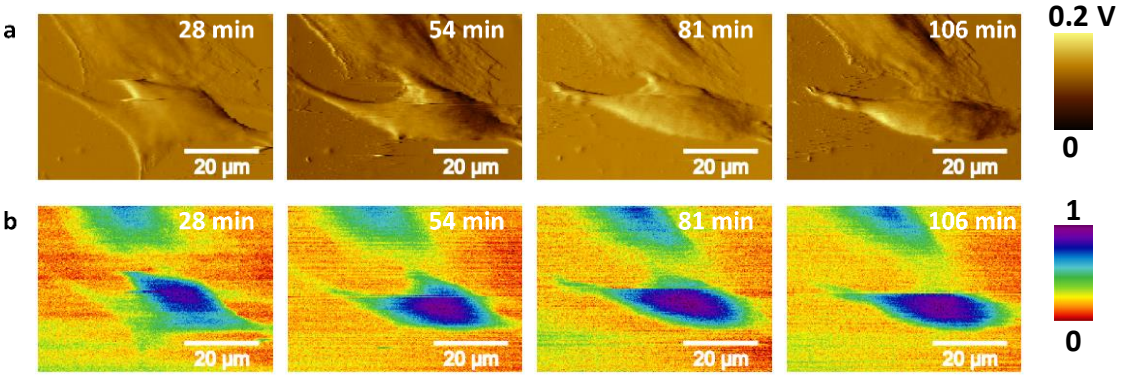

Fig. 7. Evolution of a mouse myoblast cell imaged by (a) AFM and (b) SMM in the D-MEM medium [51]. In (b), color scale indicates the normalized phase of the reflection coefficient.

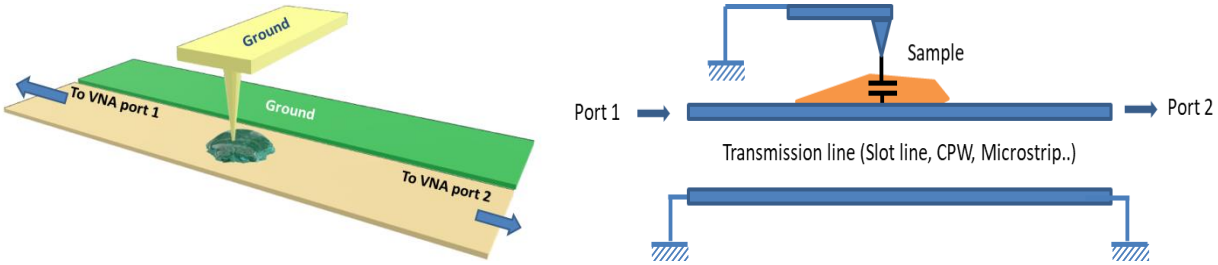

(a) (b)

Fig. 8. (a) Schematics and (b) equivalent circuit of an iSMM with a grounded AFM probe scanning a sample on top of the active electrode of a slot line [52]. The sample acts as a capacitive load on the transmission line with a ground path through the AFM probe.

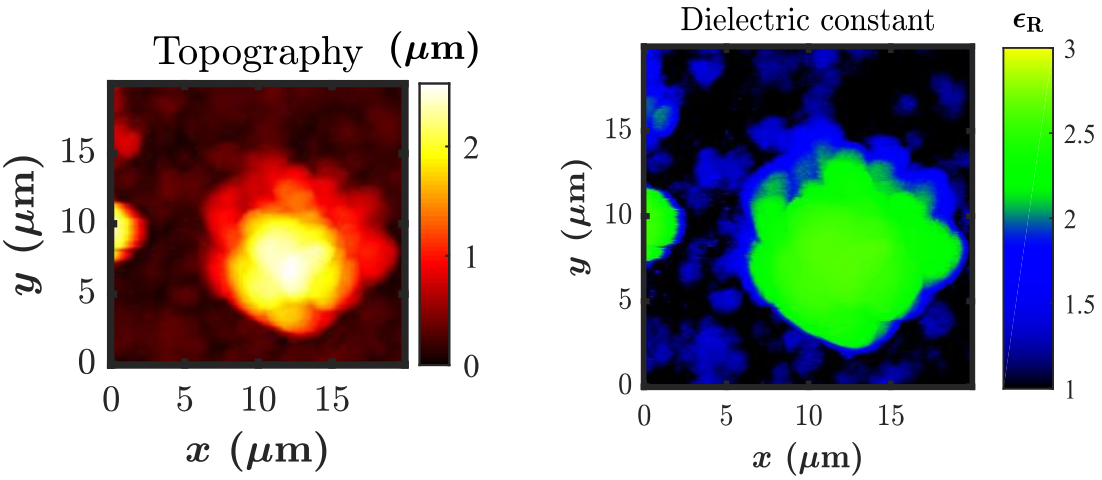

Fig. 9. (a) AFM topography and (b) iSMM dielectric-constant images of a dried human lymphocyte cell [53].